International Journal of Latest Engineering and Management Research (IJLEMR)
ISSN: 2455-4847
www.ijlemr.com || Volume 11 – Issue 03 || March 2026 || PP. 33-41

Research on the Integrated Scale-Inhibition Fracturing Fluid System with Ultra-High Salt Tolerance for Deep Coalbed Methane

Shiwen Jia[1,2], Shuangjin Zheng[1], Liangwei Xu[2], Wei Han[2], Zhiwei Yu[2]
[1]*School of Petroleum Engineering, Yangtze University, Wuhan, Hubei 434023, China*
[2]*Fracturing Company, Great Wall Drilling Co. Ltd., CNPC, Panjin, Liaoning 124010, China*

Abstract: To address the low reuse efficiency of high-salinity flowback fluid, the poor salt tolerance of conventional thickeners, and the scaling tendency of flowback fluid in tubing strings in deep coalbed methane reservoirs, flowback fluid from a coalbed methane well in Shanxi was selected as the study object. Its water quality and scaling characteristics were systematically analyzed, and a functional dry-powder slickwater system with high salinity tolerance was developed. The results showed that the dry powder dissolved rapidly in brine with a salinity of 200,000 mg/L at room temperature, with a swelling ratio of 90% within 5 min. At a dosage of 0.3%, the drag-reduction rate reached 73.6%, indicating the best overall performance. After continuous shearing at 60 °C for 90 min, the viscosity remained at 27.3 mPa·s, meeting the requirements of field fracturing operations. Complete gel breaking was achieved within 90 min using 500 ppm APS as the breaker. For $CaCO_3$-dominated scale, the selected scale inhibitor achieved a maximum inhibition efficiency of 88.5% at a broken-fluid/formation-water ratio of 2:1.

Keywords: deep coalbed methane; high salinity; scale inhibition; integrated Scale-Inhibition Fracturing Fluid

I. Introduction

As China's most resource-rich province for coalbed methane (CBM), Shanxi possesses geological resources of CBM buried below 2000 meters reaching 8.31 trillion cubic meters, accounting for nearly one-third of the national total. Among these, the development potential of deep CBM (burial depth > 1500 m) is particularly enormous [1]. However, with the large-scale development of deep CBM, the efficient reuse of flowback fluid has become a critical bottleneck in improving development efficiency, especially for high-salinity (TDS > 200,000 mg/L) flowback fluid. Due to differences in water quality from various formations during fracturing and the use of multiple chemical additives, the composition of flowback fluid is complex and highly variable [2-4]. If improperly handled during reinjection into the reservoir, it may be incompatible with formation water, leading to scaling and causing reservoir damage, thereby affecting well productivity [5,6]. Traditional polyacrylamide-based fracturing fluids are prone to precipitation with high-valence ions such as Ca^{2+} and Mg^{2+} in high-salinity environments, leading to thickening failure and deteriorated rheological properties, severely impacting fracturing effectiveness [7]. Furthermore, conventional emulsion polymer fracturing fluids not only cause high reservoir damage but also contain oil contaminants, making it difficult to meet environmental requirements. Therefore, developing a functional powdered thickener with rapid solubility, high salt tolerance, and low formation damage characteristics is crucial for realizing the resource utilization of deep CBM flowback fluid.

Addressing the application requirements of slickwater fracturing fluids, this study optimized molecular structure design, using acrylamide (AM), acrylic acid (AA), and 2-acrylamido-2-methylpropane sulfonic acid (AMPS) as the main chain monomers, and innovatively introduced the salt-tolerant monomer SPO-10. This monomer combines hydrophilic ethylene oxide (EO) chains with hydrophobic long-chain alkane structures, utilizing hydrophobic association to enhance polymer stability in high-salinity environments. A functional dry powder thickener was prepared via free radical aqueous solution polymerization. Its unique molecular network structure effectively resists salt ion erosion while maintaining excellent solubility and rheological properties. This system can not only adapt to high-salinity flowback fluid of 200,000 mg/L but also achieve a low-viscosity friction reduction rate >70%, providing an innovative solution for efficient deep CBM development. Addressing the scaling issue primarily composed of $CaCO_3$, the research indicates that under a ratio of broken gel to formation water of 2:1, the employed scale inhibitor can effectively prevent scaling, achieving a maximum scale inhibition rate of 88.5%. This system effectively solves the challenge of reusing high-salinity flowback fluid in deep CBM development and offers an innovative solution for efficient development, demonstrating broad application prospects.

II. Experimental Section

2.1 Main Materials and Instruments

Main materials: acrylamide (AM), acrylic acid (AA), and 2-acrylamido-2-methylpropane sulfonic acid (AMPS) (analytical grade, Chengdu Kelong Chemical Reagent Co., Ltd., China); OP-10, dichloromethane, acryloyl chloride, triethylamine, sodium bicarbonate, sodium hydroxide, V50, anhydrous ethanol (Chengdu Kelong Chemical Reagent Co., Ltd., China); flowback water, taken from on-site fracturing flowback fluid in Shanxi.

Main instruments: FA2004B precision electronic balance (Shanghai Youke Instrument Co., Ltd., China); ZNN-D6B electric six-speed viscometer (Qingdao Tongchun Petroleum Instrument Co., Ltd., China); DZF-6050 vacuum drying oven (Beijing Zhongxing Weiye Instrument Co., Ltd., China); SYP glass constant temperature water bath, (Gongyi Yuhua Instrument Co., Ltd., China); HAMZ-IV working fluid friction reduction evaluation experimental device, (Hai'an County Petroleum Scientific Research Instrument Co., Ltd., China).

2.2 Preparation of Functional Dry Powder

Rigid structural units and hydrophobic monomers were introduced into the polymer chains to improve salt tolerance, shear resistance, and solubility, thereby enabling both rapid dissolution and efficient drag reduction.

2.2.1 Synthesis of Functional Dry Powder SRY

Figure 1 shows the synthesis route of the salt-tolerant monomer SPO-10. First, 10 mmol of OP-10 was dissolved in 100 mL CH_2Cl_2 and transferred to a 250 mL flask. The flask was placed in an ice bath, and the mixture was stirred at 450 rpm for 30 min. Then, 50 mL CH_2Cl_2 containing 10 mmol acryloyl chloride and 12 mmol triethylamine was added dropwise, and the mixture was allowed to react under an N_2 atmosphere at 0 °C for 24 h. After the reaction, the mixture was pressure-filtered to remove triethylamine hydrochloride. The filtrate was transferred to a 500 mL separatory funnel and washed three times with saturated $NaHCO_3$ solution. The organic phase was then concentrated under reduced pressure to remove CH_2Cl_2, yielding SPO-10 as a brownish-yellow viscous liquid.

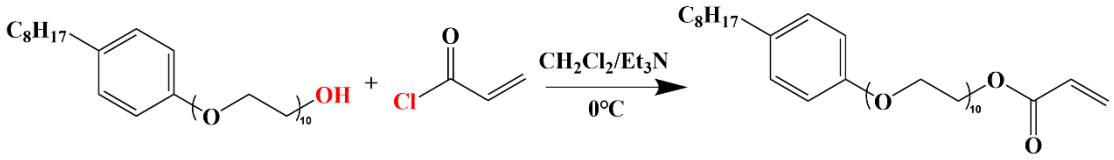

Figure 1: The Synthesis Route of the Salt-tolerant Monomer SPO-10

Using AM, AMPS, AA, and the synthesized salt-tolerant monomer SPO-10 as monomers, the salt-tolerant polymer SRY was prepared by free-radical aqueous-solution polymerization, as illustrated in Figure 2. Specifically, AM, AMPS, AA, and SPO-10 were sequentially added, in the designed proportions, to a reaction vessel containing deionized water and stirred until homogeneous. The pH of the solution was adjusted with NaOH, followed by the addition of an aqueous solution of initiator V50. After purging with nitrogen for 20 min, the reactor was sealed and placed in a water bath for polymerization at a specified temperature for a certain period, producing a gel-like product. After cooling to room temperature, the product was purified with anhydrous ethanol, cut into pieces, dried, and ground to obtain powdered SRY.

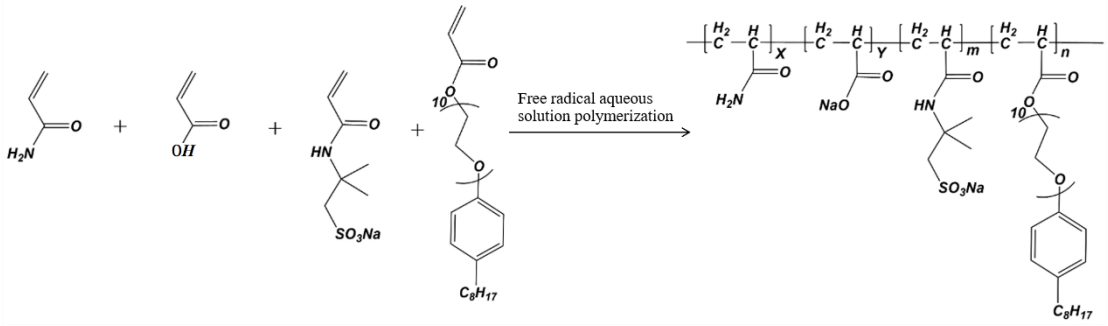

Figure 2: The Reaction Equation of Functional Dry Powder SRY

Based on single-factor optimization of the polymerization conditions, the optimal synthesis conditions for functional dry powder SRY were determined to be as follows: an AM/AA/AMPS mass ratio of 90:8:2, SPO-

10 dosage of 2% of the total monomer mass, initiator dosage of 0.06 wt% of the monomer mass, monomer concentration of 20 wt%, reaction temperature of 50 °C, pH 6.5, and reaction time of 5 h

2.2.2 Structural Characterization of Functional Dry Powder SRY

The structure of the salt-tolerant powder SRY was characterized by FT-IR and ^{1}H NMR spectroscopy. FT-IR analysis (Figure 3a) further verified the chemical composition of SRY: 3421 cm^{-1} (N-H stretching vibration of AM), 1672 cm^{-1} (C=O stretching vibration), and 1116 cm^{-1} (-SO_3^- vibration of AMPS) confirmed the presence of hydrophilic groups; 2929 cm^{-1} (-CH_2- stretching vibration) and 1558 cm^{-1} (-COO^- vibration of AA) were consistent with the polymer backbone and side-chain structure. Additionally, 1187 cm^{-1} (C-O-C of SPO-10) and 1610 cm^{-1} (benzene ring skeleton vibration) indicated the successful incorporation of the hydrophobic monomer. ^{1}H NMR analysis (Figure 3b) showed proton signals at 2.34 ppm (main chain -CH_2-), 2.22 ppm (main chain -CH-), 1.77 ppm (main chain -CH_2-), and 1.66 ppm (main chain -CH-), confirming the polymer backbone structure; the signal at 1.49 ppm was attributed to -CH_3 in AMPS. Furthermore, characteristic peaks at 6.27 ppm (benzene ring protons), 3.36 ppm (hydrophilic groups of EO chain), and 1.17--1.21 ppm (-(CH_2)n-) indicated the successful introduction of the target structure.

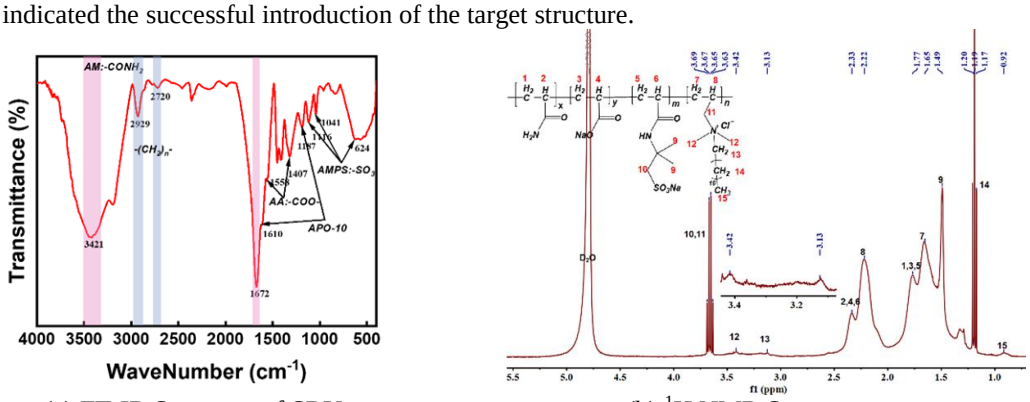

(a) FT-IR Spectrum of SRY (b) ^{1}H NMR Spectrum

Figure 3: The FT-IR Spectrum and ^{1}H NMR Spectrum of SRY

2.2.3 Micromorphology

Observation of the micromorphology of the polymer network structure at different salt concentrations via scanning electron microscopy revealed that the addition of salt ions produces an electrostatic shielding effect on the polymer molecular chains, causing them to coil and simultaneously disrupting the associative structures between chains[8]. However, SRY, relying on its strong hydrophobic association, was able to maintain a relatively intact network structure even at high salt concentrations (200,000 mg/L). This indicates that the association ability between hydrophobic chains of SRY is significant, enabling it to form a stable three-dimensional network even at low polymer concentrations, effectively resisting salt ion erosion, and thus exhibiting excellent high-salinity tolerance.

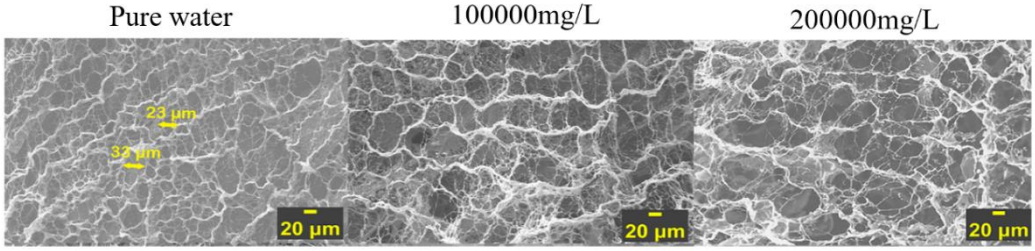

Figure 4: Micro-morphology of Fracturing Fluid in Aqueous Solution and Different Salt Concentrations

III. Performance Evaluation of Functional Dry Powder Slickwater System

3.1 Swelling Performance

The experimental results show that the high-salinity-tolerant fracturing fluid exhibits excellent dissolution performance in brine with a salinity of 200,000 mg/L. At dry-powder concentrations of 0.1%, 0.3%, and 0.5%, the swelling rates reached 85%, 80%, and 80%, respectively, within 3 minutes, and all approached 90% within 5 minutes. The viscosity increased gradually with swelling time and reached a maximum after 30-60 minutes, with values of 5, 20, and 33 mPa·s at concentrations of 0.1%, 0.3%, and 0.5%, respectively. These results indicate that the fracturing fluid has good dissolution and swelling behavior and can meet the requirements of on-site continuous mixing operations.

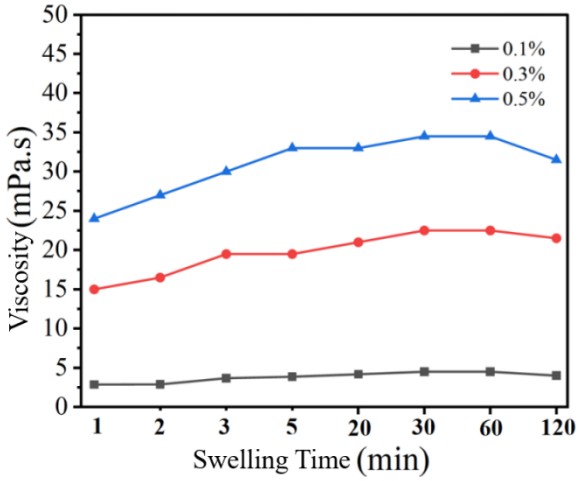

Figure 5: Dissolution Performance of High-salinity-tolerant Fracturing Fluid

3.2 Rheological Properties

The high-temperature rheological test results showed that the 0.6% high-salinity-tolerant fracturing fluid demonstrates good temperature resistance and shear resistance under 200,000 mg/L salinity conditions. After continuous shearing at 60°C and a shear rate of 170 s^{-1} for 90 minutes, the system still maintained a viscosity of 27.3 mPa·s, indicating that the polymer fracturing fluid can effectively resist thermal degradation and mechanical shear, possessing high molecular chain stability, making it suitable for high-temperature and high-shear conditions.

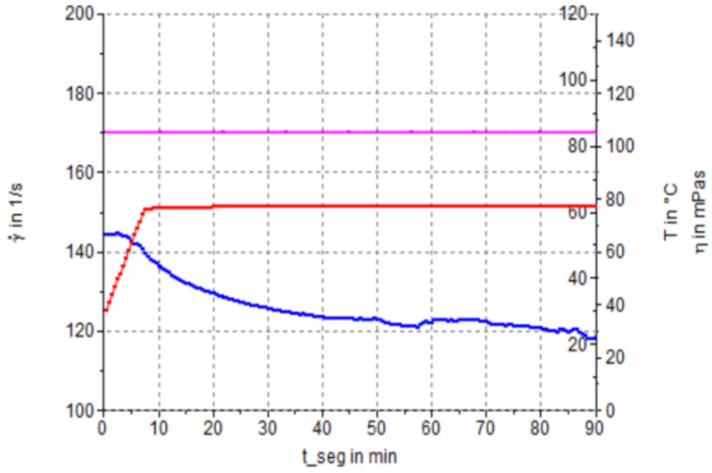

Figure 6: Apparent Viscosity Variation of Fracturing Fluid after shearing at 60℃ and 170 s^{-1} for 90 min

3.3 Friction Reduction Performance

As the concentration of the salt-tolerant polymer increased from 0.1% to 0.6%, the the viscosity of the system increased significantly, but the friction reduction rate showed a trend of first increasing and then decreasing. When the concentration increased to 0.3%, the drag-reduction rate rose from 71.3% to 73.6%, indicating that an appropriate increase in polymer concentration can optimize the friction reduction effect. However, .further increases in concentration led to a gradual decline in drag-reduction efficiency. This is attributed to the enhanced hydrophobic association between polymer molecular chains at excessively high concentrations, leading to increased fluid flow resistance. Therefore, 0.3% was identified as the optimal dosage, at which the maximum drag-reduction rate of 73.6% was obtained.

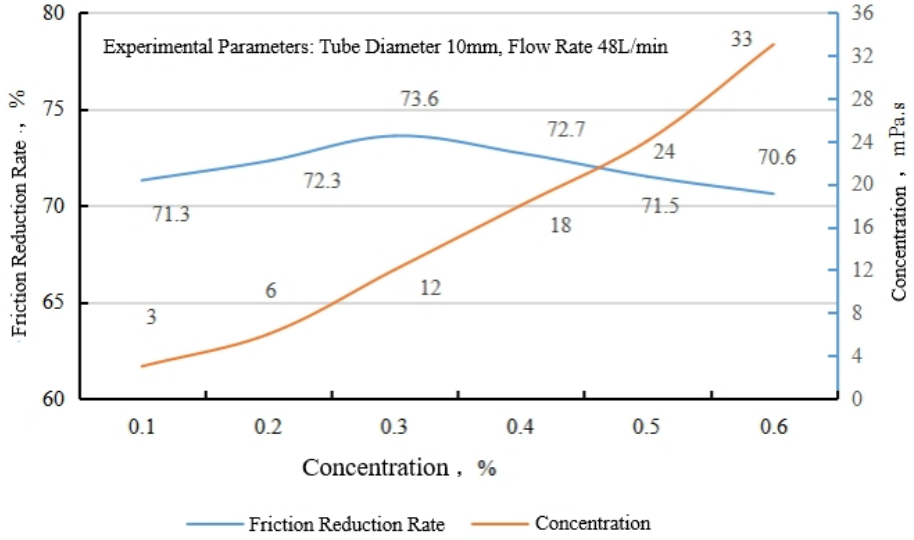

Figure 7: Viscosity and Friction Reduction Rate of Fracturing Fluid at Different Additive Concentrations

3.4 Proppant Carrying Performance

High-salinity-tolerant fracturing fluids of different concentrations were prepared using simulated brine with a salinity of 200,000 ppm. The settling time of the proppant in the fracturing fluid was tested in a 100 mL graduated cylinder. The proppant used was 40/70 mesh quartz sand at a 20% sand ratio. The test results are shown in Table 1.

Table 1: Test Results of Sand Suspension for Fracturing Fluids at Different Concentrations Using Simulated Brine

Ratio	Gelling agent concentration0.1%	Gelling agent concentration0.3%
Settling time of proppant(s)	15	95

Figure 8: Proppant Carrying Capacity of Slickwater with Different Functional Dry Powders

The test results indicate that at low concentration conditions (<0.1%), the proppant carrying performance of the example slickwater showed no significant difference compared to the comparative example. However, with increasing thickener concentration, the proppant carrying capacity significantly enhanced. When the dry powder concentration increased from 0.1% to 0.3%, the proppant carrying time for 20% sand ratio (40/70 mesh quartz sand) was substantially extended from 15s to 95s, indicating a significant optimization in the system's viscoelasticity and suspension capacity. At a concentration of 0.3%, the proppant carrying performance of the high-salinity-tolerant fracturing fluid was sufficient to meet field operational requirements.

3.5 Gel Breaking Performance

The experiments show that the gel breaking performance of the 0.3% thickener + 0.05% APS system differs in fresh water and high-salinity brine (200,000 mg/L). The fresh-water fracturing fluid showed better broken-fluid properties, with a viscosity of 1.52 mm2/s, a surface tension of 27.115 mN/m, and a residue content of 8.132 mg/L. In contrast, the high-salinity system broke faster, but the broken gel parameters were

slightly higher (viscosity 2.01 mm²/s, surface tension 28.362 mN/m, residue 13.537 mg/L). The results indicate that high salinity accelerates gel breaking but slightly affects the quality of the broken gel, which overall still meets operational requirements.

Table 2: Test Results of Gel Breaking Performance

Fracturing fluid type	Temp (℃)	APS dosage (ppm)	Gel breaking time (min)	Viscosity of broken gel (mm^2/s)	Surface tension of broken gel(mN/m)	Residue content of broken gel(mg/L)
Clear water fracturing fluid	70	500	60	1.52	27.115	8.132
High salinity resistant fracturing fluid	70	500	90	2.01	28.362	13.537

IV. Study on Scale Inhibitor for High-Salinity Slickwater

Fracturing is a widely used stimulation technique in oil and gas reservoirs.However, its application alters the temperature and pressure distribution within the formation, disrupting the equilibrium of formation water and leading to scaling issues, particularly the deposition of calcium carbonate[9-11]. In addition, when fracturing fluid penetrates the formation, if its composition is incompatible with the formation water, it can also induce scaling, blocking pores and affecting stimulation results. Therefore, recycling and reuse of fracturing fluid can not only reduce production costs but also effectively minimize environmental pollution and water resource wastage[12]. For a long time, the presence of large amounts of low-solubility inorganic salts in pipelines often leads to the formation of inorganic salt scale on pipe surfaces, causing pipeline damage and increasing production costs[13]. Conventional scale inhibitors and scale-inhibition systems are often unable to satisfy the salinity-tolerance requirements associated with soluble-salt scaling in deep unconventional reservoirs. Therefore, it is necessary to develop scale inhibitors suitable for such conditions. In this study, the optimization and performance evaluation of scale inhibitors in high-salinity fracturing fluids were investigated to explore scale-control technology suitable for deepCBM fracturing.

4.1 Analysis of Deep CBM Flowback Fluid Properties

Two samples of on-site flowback fluid from CBM Well M were collected and allowed to stand at room temperature for 30 days. The upper layer was a clear saturated solution, while solid salt scale precipitated in the lower layer (Figure 9). The clear saturated solution of upper layer was analyzed using the dual-indicator titration method and atomic absorption spectrophotometry. The results are shown in Table 3. It can be seen from Table 3 that the maximum salinity is 2.2×10^5 mg/L.

Table 3: Analysis Results of Ion Content in Two Flowback Fluids

Flowback Water Samples	Ion Content，mg/L					Salinity，mg/L
	Cl^-	Na^+	Mg^{2+}	Ca^{2+}	Fe^{3+}	
Sample 1	94970.5	8620.17	3289.16	22361.43	536.67	170000
Sample 2	115464.2	8967.33	4573.77	31164.53	762.39	220000

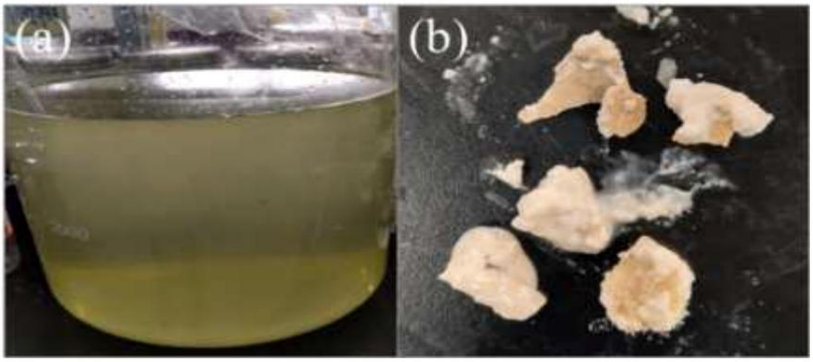

Figure 9: (a) Supernatant of Coalbed Methane Flowback Fluid (b) Scale Sample

4.2 Analysis of Salt Scale Composition

Salt scale samples from a CBM well in Shanxi were first collected. The salt scale was dried in a vacuum drying oven (0.09 MPa, 45 °C) and ground. The composition and elemental characteristics of the scale were then analyzed by SEM-EDS and XRD to determine its mineralogical composition.

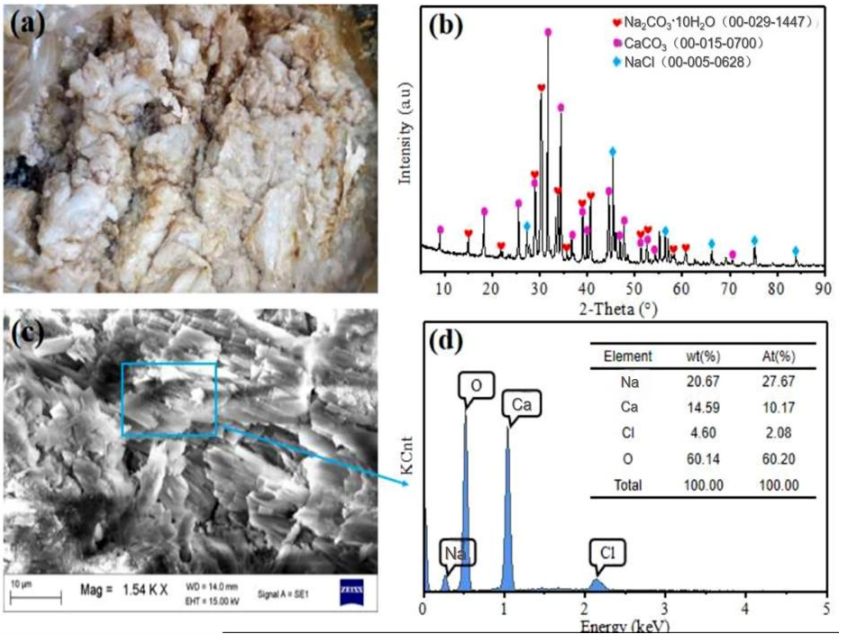

Figure 10: (a) Original Scale Sample (b) XRD (c) SEM (d) EDS

The experimental results are shown in Figure 10. AS indicated by the XRD pattern in Figure 10(b) the major diffraction peaks of the salt scale match those of sodium carbonate and calcium carbonate. Some individual diffraction peaks correspond to the XRD pattern of sodium chloride, suggesting the possible presence of a small amount of sodium chloride in the salt scale. Figure 10(d) shows that the main elements of this salt scale are Ca, O, Cl, and Na. Comprehensive analysis suggests that the salt scale exists as a composite of calcium carbonate, sodium carbonate, and sodium chloride. Analysis of the on-site scale sample by SEM-EDS and XRD showed that the main component of the scale layer is $CaCO_3$, followed by small amounts of NaCl and sodium carbonate. Therefore, this study subsequently focuses on evaluating the performance of scale inhibitors for calcium carbonate scale inhibition.

4.3 Scale Inhibitor Selection and Performance Comparison

According to the industry standard SY/T5673-2020, General Technical Conditions of Scale Inhibitor for Oil Fields,, the scale inhibition capability of scale inhibitors with different molecular structures against calcium carbonate was investigated. First, the performance of four types of single scale inhibitors was compared. They were heated and allowed to stand at 70°C for 16 hours, with a scale inhibitor addition concentration of 100 ppm. The results are shown in Table 4 and Figure 11.

Table 4: Antiscale Efficiency of Four Different Scale Inhibitors

Scale inhibition type	Sample	Average volume of EDTA consumed（mL）	Scale inhibition rate（%）
Calcium carbonate scale inhibition	Blank group 1	19.53	/
	Blank group 2	12.30	
	Scale inhibitor No. 1	16.93	64.06
	Scale inhibitor No. 2	18.95	91.98
	Scale inhibitor No. 3	18.33	83.40
	Scale inhibitor No. 4	19.2	95.44

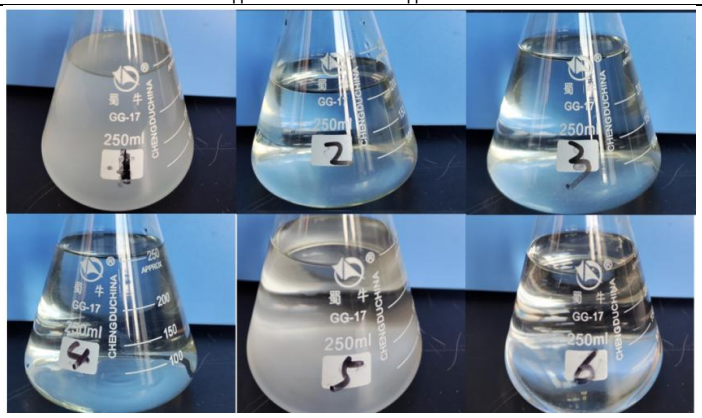

Figure 11: Photographs of Specimens after Heating
(No. 1–4: Four different scale inhibitors; No. 5–6: Blank groups)

As shown in Table 4, all four scale inhibitors have a certain inhibitory effect on calcium carbonate scale, but the effectiveness varies: Scale Inhibitor No. 1 showed the poorest inhibition effect; Scale Inhibitors No. 2 and No. 3 performed well; Scale Inhibitor No. 4 had the optimal effect, achieving an inhibition rate of up to 95.4% for calcium carbonate scale. Considering the above results and the composition of the scale layer, Scale Inhibitors No. 2, No. 3, and No. 4 were prioritized for subsequent research related to high-salinity slickwater.

4.4 Formulation Optimization of Scale-Inhibiting Slickwater System

To investigate the effects of gel breaking and the functional dry powder on scale-inhibition performance, formation water was mixed with the broken fluid from the scale-inhibiting fracturing fluid at ratios of 1:2, 1:1, and 2:1. The scale-inhibition performance was evaluated at 90 °C to optimize the formulation of the slickwater system[14]. The experimental results are shown in Figure 12.

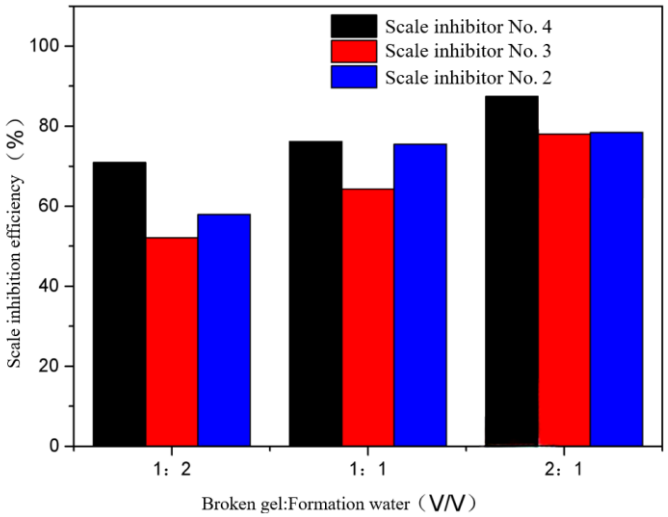

Figure 12: Scale Inhibition Rate of Broken Gel Mixed with Formation Water in Different Ratios
(Scale inhibitor dosage: 100 mg/L)

Comparing Table 4 and Figure 12, it can be seen that when the scale inhibitor is added to the slickwater system, subjected to gel breaking treatment, and then mixed with formation water, its scale inhibition efficiency is lower than that of the single scale inhibitor alone. This is because ammonium persulfate is used for oxidative gel breaking during the process, which can cause some damage to the molecular structure of the scale inhibitor[15].

Simultaneously, as the proportion of broken gel increases, the scale inhibition efficiency of all three scale inhibitors shows a gradually rising trend. Under different ratios of broken gel to formation water, these three scale inhibitors all exhibited certain scale inhibition performance. Among them, Scale Inhibitor No. 4 demonstrated the best scale inhibition effect when the ratio of broken gel to formation water was 2:1, achieving a scale inhibition rate of up to 88.5%. Considering all factors, Scale Inhibitor No. 4 was selected for the formulation of the scale-inhibiting slickwater system, at a concentration of 100 mg/L.

V. Conclusions

(1) The developed system possesses excellent salinity tolerance and operational performance. The functional dry-powder slickwater system dissolved rapidly in brine with a salinity of up to 200,000 mg/L, achieving a swelling ratio of 90% within 5 min. At a dosage of 0.3%, the drag-reduction rate reached 73.6%, and the viscosity remained at 27.3 mPa·s after shearing at 60 °C for 90 min, demonstrating good thickening ability, drag-reduction performance, and shear resistance.

(2) The system also showed excellent scale inhibition performance and complete gel breaking. Targeting the $CaCO_3$ scaling issue in high-salinity flowback fluid, the optimized Scale Inhibitor No. 4 achieves a scale inhibition rate of 88.5% at a broken gel to formation water ratio of 2:1. In addition, complete gel breaking was achieved within 90 min using 500 ppm APS, and the properties of the broken fluid met operational requirements.

(3) The ultra-high salt tolerant integrated scale-inhibition fracturing fluid system was validated through laboratory evaluation and, showed good operability and economic benefits for on-site reuse of deep CBM flowback fluid. Therefore the system possesses excellent potential for widespread application and provides a reliable technical means for fracturing stimulation in similar reservoirs.

References

[1]. XU Hao, TANG Dazhen, TAO Shu, et al. Differences in geological conditions between deep and shallow coalbed methane and their formation mechanisms [J]. Coal Geology & Exploration, 2024, 52(2): 33-39.

[2]. YUAN Shiyi, HAN Haishui, WANG Hongzhuang, et al. Research progress and prospects of new methods for enhanced oil recovery in oilfield development [J]. Petroleum Exploration and Development, 2024, 51(4): 841-854.

[3]. CHEN Gang, WANG Weilong, YANG Shuisheng, et al. Treatment and reuse technology of fracturing flowback fluid in Wuqi Oilfield and its application [J]. Industrial Water Treatment, 2025, 45(2): 175-183.

[4]. HE Dandan, LAI Lu. Research progress on technology of preparing water-based fracturing fluid from oil and gas field wastewater [J]. Industrial Water Treatment, 2024, 34(6): 1-17.

[5]. LESTER Y, FERRER I, THURMAN E M, et al. Characterization of hydraulic fracturing flowback water in Colorado: Implications for water treatment [J]. Science of the Total Environment, 2015, (4): 637-644.

[6]. EDIRISINGHE E A A V, PERERA M S A, ELSWORTH D, et al. Particle transport in fractured geo-energy reservoirs considering the effect of fluid inertia and turbulent flow: A review [J]. Journal of Rock Mechanics and Geotechnical Engineering, 2025, 17(3): 1906-1939.

[7]. XU Bing, ZHANG Qian, WU Huanhuan, et al. Integrated membrane process of tubular ultrafiltration-nanofiltration-electrodialysis-reverse osmosis for treating fracturing flowback fluid [J]. Journal of Cleaner Production, 2024, 469 (1): 142995.

[8]. ZHANG Xiaoxin, LAI Xiaojuan, TANG Meirong, et al. Preparation and properties of temperature-resistant and salt-tolerant emulsion fracturing fluid thickener [J]. Applied Chemical Industry, 2022, 5(2): 455-459.

[9]. XU Shijing. Reservoir damage mechanism during stimulation in tight sandstone oil reservoirs [J]. Science Technology and Engineering, 2019, 19(23): 92-99.

[10]. YOU Lijun, XIE Benbin, YANG Jian, et al. Damage mechanism of fracturing fluid flowback to reservoir fractures in shale gas wells [J]. Natural Gas Industry, 2018, 38(12): 61-69.

[11]. Sun H, Kim J, Gomaa A M, et al. High-Temperature Fracturing Fluid with Seawater: Economical Control for Precipitation and Scale [C]. the SPE Asia Pacific Hydraulic Fracturing Conference, Beijing, SPE-181832-MS.

[12]. LYU Lei, WANG Zimin, YANG Zhigang. Problems and countermeasures in the treatment and reuse of shale gas fracturing flowback fluid [J]. Chinese Journal of Environmental Engineering, 2017, 11(02): 965-969.

[13]. WANG Gaihong, LIAO Lejun, GUO Yanping. Development and application of a recoverable clean fracturing fluid [J]. Drilling Fluid & Completion Fluid, 2016, 33(06): 101-105.

[14]. CHEN Huaxing, SHEN Jianjun, LIU Yigang, et al. Evaluation method for scaling tendency between injected water and formation water in oilfields [J]. Oilfield Chemistry, 2017, 34(2): 367-373.

[15]. Yan Lianhe. Manual of water treatment agents and formulations [M]. China Petrochemical Press, 2004.